

Using satellite imagery to monitor remote rural economies at high frequency

Tillmann von Carnap^{1*}, Reza M. Asiyabi^{2,3}, Paul Dingus¹, Anna Tompsett^{4,5}

Affiliations:

¹ Center on Food Security and the Environment, Stanford University; Stanford, 94305, United States of America.

² Mistra Center for Sustainable Markets, Stockholm School of Economics; Stockholm; 11350; Sweden

³ School of GeoScience, University of Edinburgh; Edinburgh; United Kingdom; EH8 9XP; United Kingdom

⁴ Beijer Institute of Ecological Economics, The Royal Swedish Academy of Sciences; Stockholm; 10405; Sweden

⁵ Institute for International Economic Studies, Stockholm University; Stockholm; 10691; Sweden

*Corresponding author. tcarnap@stanford.edu

Despite global progress in reducing extreme poverty, stubborn pockets remain, often in remote and fragile regions. A fundamental obstacle to further progress is that remoteness and fragility also constrain our ability to monitor economic conditions. Using satellite imagery, we develop a new approach to monitor economic activity at periodic markets, focal points for rural trade throughout history and much of the world today. We describe how to detect marketplaces without pre-existing maps and how to construct an up-to-weekly measure of their activity. We show that we successfully detect marketplaces and that activity correlates with other measures of economic activity, captures seasonal patterns, and responds to local weather and conflict. Drawing on high frequency, globally available imagery, our approach enables real-time monitoring of economic activity independent of ground conditions.

Following an extraordinary reduction in global poverty over the last century (1), progress in eliminating extreme poverty has slowed. Recent figures show that the number of people in extreme poverty has risen in sub-Saharan Africa (2-3). Globally, remaining pockets of poverty are increasingly concentrated in remote, or fragile and conflict-affected areas (4).

A central barrier to alleviating poverty in these contexts is that remoteness and fragility affect both economic outcomes and our ability to monitor them (5). Remoteness and fragility make it costly, or impossible, to collect field data or maintain consistent administrative records. The resulting lack of accurate and timely data is particularly problematic during critical periods such as conflict, natural disasters, or epidemics, preventing policymakers from detecting deteriorating conditions in time to intervene and limiting researchers' ability to identify mitigating interventions.

To fill this gap, we propose a novel method to remotely monitor activity in rural marketplaces. Since at least the Roman Era (6), rural marketplaces have facilitated trade between farmers selling their crops, households shopping for daily needs, and merchants sourcing and supplying products (7-8). Busier market days reflect more local economic activity: more income to be spent, more goods to be traded, or both. Crucially, markets typically take place in the open, making them visible in high-resolution satellite imagery and allowing their activity to be tracked over time.

Tracking rural marketplaces with satellite imagery presents unique advantages for monitoring remote economies. Other sources of information on economic conditions, such as household surveys, are infrequently collected, spatially sparse, and costly to scale. In contrast, satellite imagery now combines high spatial resolution with dense geographical and temporal coverage (9-10). Absent cloud cover, satellites capture near-daily images of every marketplace worldwide. Satellites also collect data continuously and consistently regardless of local conditions, ensuring comparability across space and time. Finally, and unlike survey data, satellite images are available

in real-time, and processing can be fully automated. This provides an unprecedented ability to monitor rapidly evolving situations.

Existing monitoring approaches using satellite imagery in low-income countries implicitly or explicitly infer conditions from large assets that are visible from space, such as buildings or infrastructure (11-12). These assets, however, change slowly. Consequently, existing approaches cannot capture real-time effects of shocks and have to date primarily informed comparisons across space or over long periods (13). In contrast, marketplace activity can visibly change every week, providing the spatial and temporal granularity needed to measure short-term changes or rapidly target assistance.

This paper demonstrates how to detect marketplaces and track their activity using globally available near-daily satellite imagery. We validate our detection method with secondary data from Kenya, Malawi, and Mozambique. We then apply the method to derive novel market maps and activity panels in Kenya and Ethiopia, two countries where periodic markets are widespread. We use the panels to illustrate the sensitivity of the activity measure to local economic changes using both survey data and responses to exogenous shocks, such as weather and conflict. Unlike existing methods, ours can produce fine-grained estimates of short-term changes in economic activity for remote rural areas, using widely accessible data.

Detecting and tracking marketplaces

To monitor marketplaces, one must first know their locations. Likely because of their geographical sparseness and informal nature, however, maps are rare. Furthermore, no consistent definition of a marketplace exists: informally, the term can describe anything from a handful of individual stalls selling small quantities of goods to large, urban wholesale operations. Beginning from a candidate location, such as a village, our approach detects markets meeting the following criteria: i) occurring

periodically (e.g., one or two market days per week); ii) at least partly taking place in the open; iii) operating sufficiently frequently between June 2016 – when imagery becomes consistently available – and September 2023 – our cutoff date – to distinguish activity from background noise; (iv) operating around 10:30 AM local time when most imagery is captured; and (v) having an open-air footprint of at least 50m².

As evident in very-high-resolution (VHR; 30cm) images from Mozambique, marketplaces appear differently on market days and non-market days (Fig. 1A). At this resolution, colourful market structures and attending crowds are clearly visible on a Sunday, the local market day, and conspicuously absent on a Wednesday.

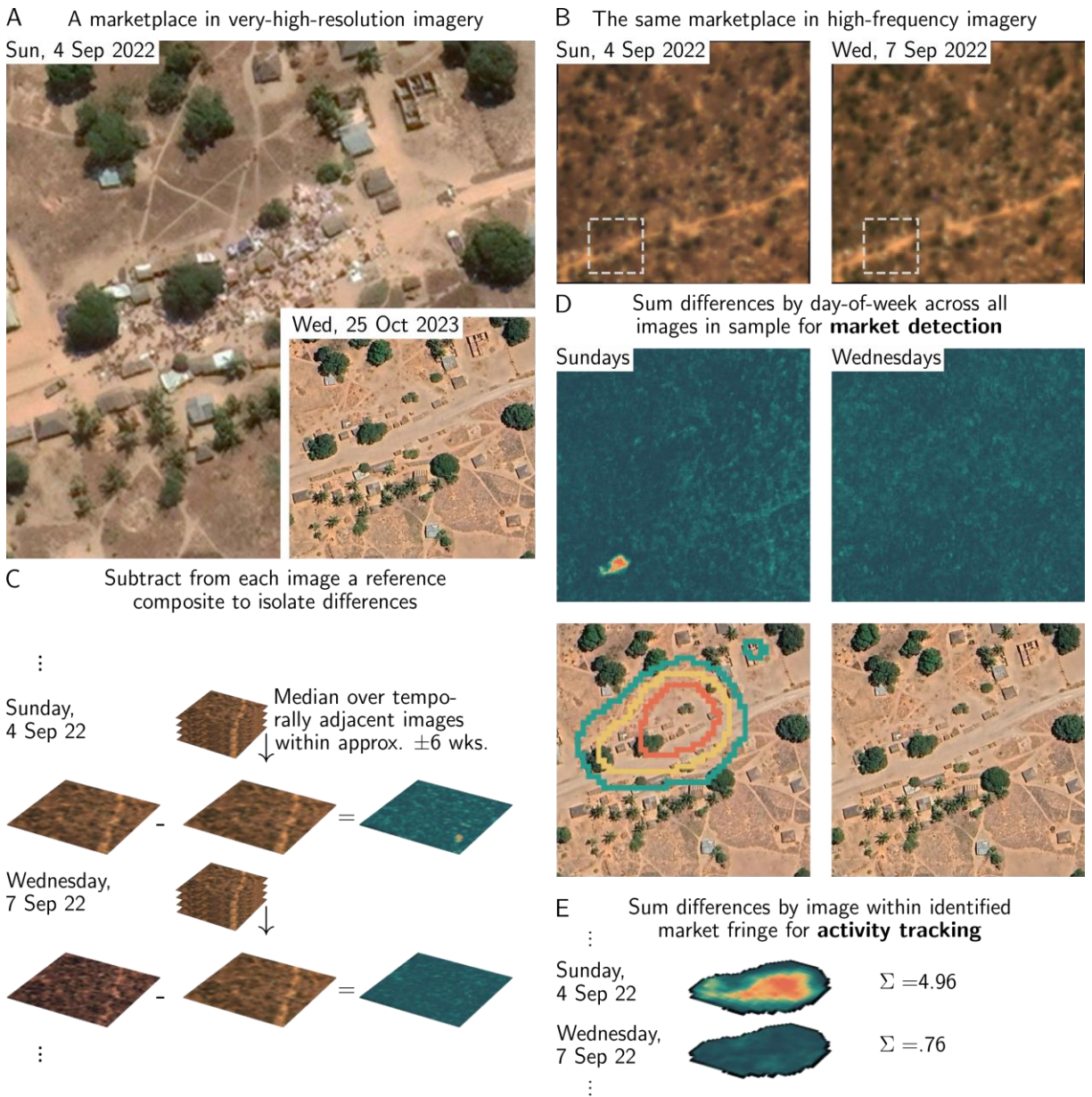


Fig. 1: Method intuition & sequence. (A) A marketplace in Nangata, Mozambique (14.21°S , 40.70°E) as seen in the Google Earth Archive on a non-market day (Wednesday) and a market day (Sunday). Market activity is discernible as crowds, stalls, and vehicles in the Sunday image. (B) The same location on a Sunday and a Wednesday in PlanetScope imagery. (C-E) Illustration of workflow for market detection and activity tracking. Individual PlanetScope images between June 2016 and September 2023 are differenced with median composites from temporally adjacent images primarily from within 6 weeks (see Materials & Methods) – approximating the appearance

on a non-market day – to isolate appearance differences due to market activity (C). Aggregate differences per day-of-week identify market shapes at various threshold levels (D). The high-resolution images show the area in which market shapes are detected at various threshold levels. Market activity readings within these shapes are derived by summing differences across pixels within each shape and image (E). We then select as the market area to consider the area and associated readings from the largest shape in which the median reading across all market days in the sample exceeds the reading at the 75th percentile across non-market days.

Acquiring such VHR imagery at scale is prohibitively expensive, however, and available images only sporadically capture market days. Instead, we use lower resolution (3.1m) PlanetScope RGB imagery (Fig. 1B) that is globally available with a median average revisit interval of 30 hours (14). In an individual Sunday image at this lower resolution, market activity is barely visible as a patch of relative darkness. We can nonetheless detect a temporal signature because, in an imagery stack, appearance differences that are associated with market activity occur *regularly*, on market days. In contrast, other appearance differences, such as those arising from the ploughing of fields or wetting of soils, occur erratically.

To detect the periodic appearance differences that characterise market activity, we would ideally use imagery from the same location on a non-market day as a reference. While we do not know market days beforehand, we build on the intuition that, if markets occur fewer than half the days in a week, a median composite of sufficiently many images will resemble a non-market day. We therefore construct for each image a reference composite using imagery from surrounding dates. Subtracting this composite yields a difference image that highlights areas that appear unusual for the given period (Fig. 1C). Averaging these difference images by day-of-week yields a representation where pixels with periodic changes on a given day-of-week exhibit higher values than those whose appearance does not vary by day-of-week (Fig. 1D).

Across marketplaces, market day activity varies in its appearance compared to non-market days. Sometimes it is brighter than the otherwise bare ground, sometimes darker; furthermore, vendors may use temporary structures of distinctive but locally idiosyncratic colours. We address this heterogeneity by aggregating the information in each pixel of each day-of-week difference image into a summary measure of brightness and colour differences. Specifically, we multiply the maximum absolute difference of values across the red, green, and blue bands – tracking brightness variation – with the maximum absolute difference of angles in a polar representation of the image (15) – tracking colour variation.

We identify contiguous areas where combined brightness and colour differences exceed predefined thresholds and tune these thresholds using ground truth data. While this procedure could potentially identify other periodic events like religious gatherings, we validate below that we indeed predominantly detect marketplaces.

We now turn to measuring activity over time. Marketplaces typically feature a core with relatively stable activity and a fringe with seasonal or other fluctuations, but their relative positions vary with market layouts. To track activity variation across heterogeneous marketplaces, we first identify each marketplace's fringe. Overlapping areas defined by successive thresholds, we create a series of concentric rings. Within each ring and for each image, we compute the mean of brightness and colour differences as above. We then define the fringe of each marketplace as the largest ring where the median measure on market days exceeds the 75th percentile of non-market days. For each image, our preferred measure of activity is the mean of the brightness and colour differences across pixels within the area constituting the outer boundary of the fringe (Fig. 1E).

Relevance and validation

For remotely-sensed market activity to constitute a relevant and valid measure of rural economic activity, the marketplaces we detect must be integral to the rural economy, detection must be accurate, and the activity measure must respond to changes on the ground. We begin by arguing that periodic markets indeed represent relevant rural trading locations and that the specific type of periodic markets our method detects – operating fewer than half of the days each week, having some activity outdoors, active around noon – constitutes the norm rather than an exception.

Available data on rural economies do not allow us to reliably calculate descriptive statistics such as the share of rural revenue generated at periodic markets, or the share of output traded there relative to other channels. Historically, however, periodic, open-air markets with dedicated market days have represented an efficient mode of organizing exchange in areas where aggregate economic activity is too low to sustain the permanent, formal operations typical of towns and cities (16). Applying our approach to Kenya and Ethiopia, we confirm that such markets remain geographically widespread (Fig. S1), suggesting their continued relevance.

Furthermore, among the 1,189 periodic marketplaces we detect in Kenya and Ethiopia, those that operate once a week (74%) are more common than more frequent ones (20% operate twice, 6% thrice; Fig. S2), suggesting persisting advantages of relatively infrequent gatherings. Also, many of the detected areas encircle what are likely fixed market structures, illustrating that even when markets are partly covered, activity spills into surrounding areas where it is detectable (Fig. S3). Finally, markets held around noon facilitate access for participants travelling from surrounding areas, while morning or evening markets primarily serve local populations, such as in more densely populated urban settings not targeted by our approach.

To evaluate how successfully we detect markets, we would ideally use up-to-date, internationally comprehensive market maps. Similarly, we would evaluate our activity measures using high-frequency local measures of economic activity. Such data largely do not exist either, however, and their absence motivates our work. Using the limited available sources of validation data, we confirm that: (i) we successfully detect known marketplaces; (ii) detected areas overwhelmingly correspond to trading locations rather than other periodic events; (iii) seasonal activity patterns correspond in sign and magnitude to ground data; and (iv) measured activity responds to weather shocks.

To validate our detection procedure, we use secondary datasets from Kenya (17), Malawi (18), and Mozambique (19) that list the coordinates and days of operation for 60, 31, and 48 marketplaces, respectively, with 1.2 market days per market on average (Fig. S4). These datasets let us directly test our ability to detect periodic markets where they are known to exist. However, we lack maps of otherwise comparable locations without marketplaces. To examine how frequently we erroneously detect markets, we use the designated non-market days as pseudo-instances of such locations. Specifically, we remove all images of designated market days for a given location from its imagery sample, replacing them with randomly sampled images from designated non-market days. The resulting sample should approximate the appearance of an otherwise comparable location without a periodic market. We then calculate the share of these pseudo-locations that are erroneously identified to have a market on any day ('false positive rate'). Within the original set of locations, we calculate the share of location-day tuples that are correctly detected ('recall') and the share of detected tuples that are designated market days for a given location ('precision').

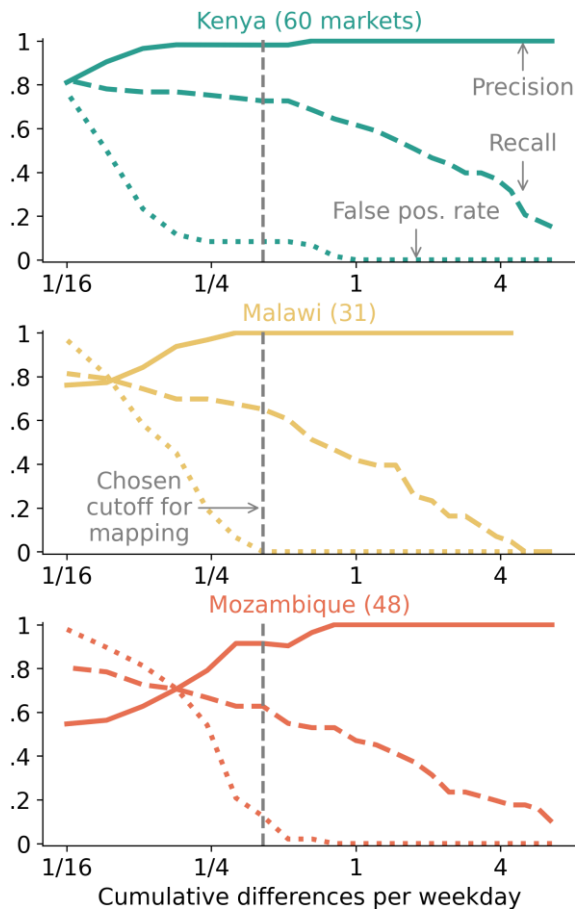


Fig. 2: Validation of market detection against ground-based marketplace maps. Precision, recall and false positive rate (the share of pseudo non-market locations for which the algorithm erroneously detects any marketplace) across market datasets from three countries. The horizontal axis indicates a range of possible threshold values at which aggregate periodic deviations would be considered a market shape. The vertical line at 0.41 identifies the chosen threshold for the mapping exercise underlying the subsequent activity analyses.

Despite varying economic and agro-ecological settings and across a broad range of the tuning parameter, we achieve precision above 90% in the sample of locations with marketplaces, and a false-positive rate below 10% in the sample of pseudo-locations without marketplaces (Fig. 2). Furthermore, the method detects markets across a range of local population densities (Fig. S5A) and marketplace sizes (Fig. S5B).

We observe lower recall rates, driven by locations where we do not detect activity on designated market days. Several factors may contribute: first, although we intentionally select datasets that list marketplaces with distinct market days, some marketplaces may have similar levels of activity on other days, complicating their detection, which potentially also affects the false positive rate. Second, some market coordinates, particularly in Mozambique, refer to large trees, which often serve as local gathering places. While periodic activity may indeed happen in the shade of these trees, it is likely on a substantially smaller scale than most of the markets we successfully detect. Finally, the datasets were collected at different times. Only markets that were active for a sufficiently large share of our imagery period will be detectable.

These factors do not reflect shortcomings of our specific validation data but intrinsic challenges when studying such a dynamic and diverse phenomenon. No current approach can detect and monitor economic hubs of *all* forms and sizes. Our approach allows detection and monitoring of a consistently defined group.

Regarding potentially misidentified marketplaces, our method demonstrates high precision at higher threshold values, as well as a low false positive rate. For lower threshold values, we can investigate false positives by overlaying detected market shapes onto VHR imagery. At the threshold chosen for the mapping exercise, we identify two cases in Kenya where livestock pens adjacent to marketplaces are detected on days immediately before or after designated market days – likely livestock brought to the market in advance or awaiting transport after sale – as well as one possible instance of a gathering in front of a public building. Overall and beyond the validation market maps, out of 1,577 detected location-by-market-day tuples in Kenya and Ethiopia, only 31 (2%) lie within 50 metres of a religious building registered in OpenStreetMap and have a signal we detect on days of worship (Tab. S1). Furthermore, although VHR imagery does not always show market activity – images may not capture market days –, the detected outlines have

consistently intuitive layouts when overlaid on such imagery, such as along roads or on village squares. Finally, when we detect multiple market days at the same marketplace, they are typically scheduled three days apart – as is characteristic among periodic markets (16) – and their centroids lie, at the median, only 29 metres apart (Tab. S2).

We now validate our market activity measure. Across exercises, we normalise all readings to average zero on non-market days and 100 on market days. Specifically, we first subtract from each reading the average non-market day activity over a reference period (see notes for Fig. 3), and then divide readings by the average of the thus-normalised market day readings over the same period. Fig. 3A provides an example for an individual marketplace over a three-week period. As for the validation of the detection approach, activity readings are markedly different on designated market days and non-market days.

We expect market activity to track economic conditions on the ground. We assess this with data from a uniquely dense ground survey of 3,539 non-agricultural, mostly informal firms in Western Kenya in early 2022 (Figs. 3B & S4) (20). Trends in activity at the 16 detected marketplaces within 5km of the firms are strikingly similar to trends in firm revenue and profit.

We further confirm that the activity measure responds to external factors that affect rural economies, such as weather. Specifically, we focus on Western Kenya as a region characterised by rainfed smallholder farming (21). In this region, a bimodal rainfall pattern induces two harvest seasons, around April and October. These agricultural cycles are mirrored in seasonal activity fluctuations in the 263 marketplaces we detect in the region. Peak activity occurs when farmers market their crops and acquire inputs for the next planting cycle (Fig. 3C).

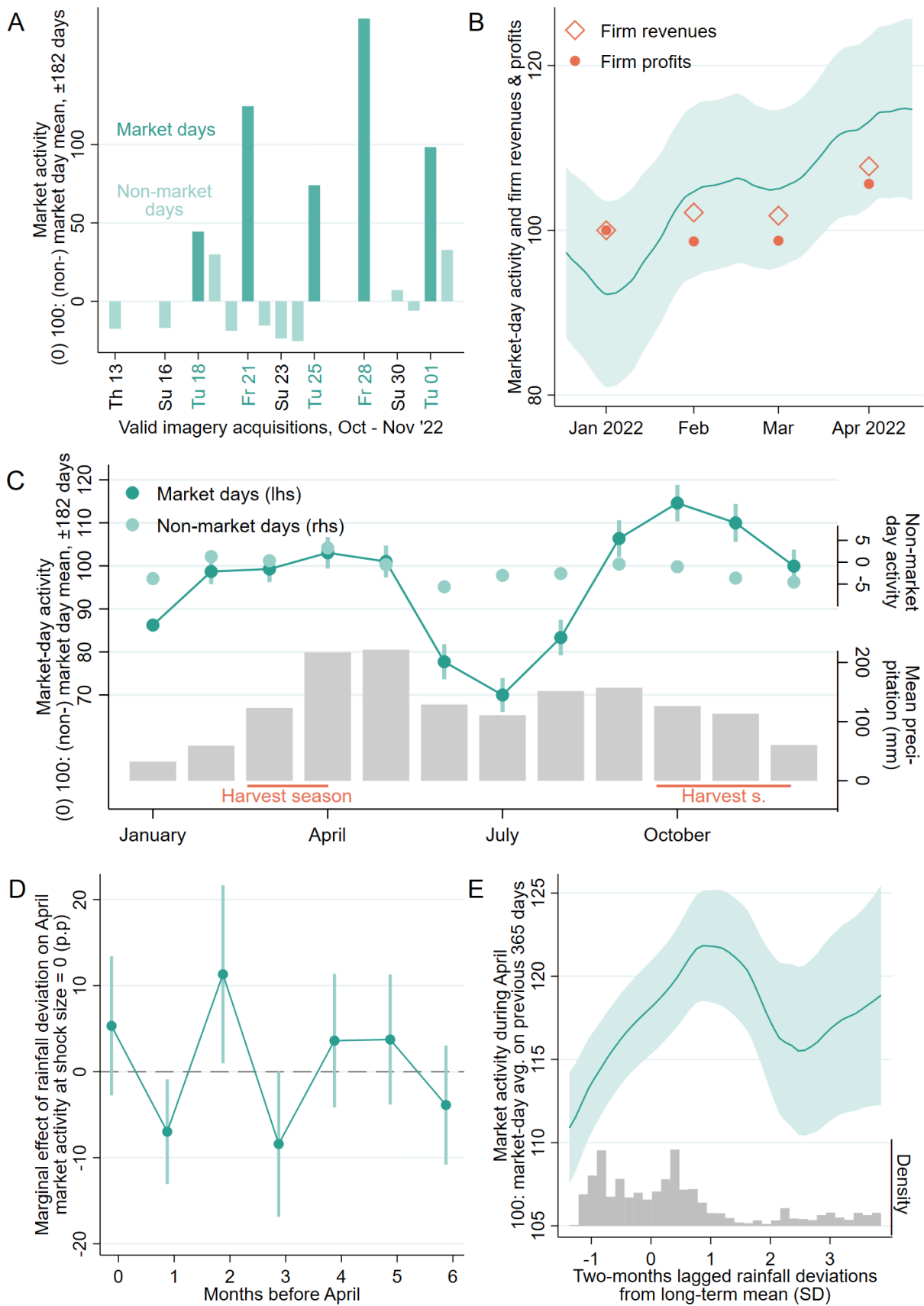


Fig. 3: Validation of activity tracking with Kenyan sample markets. (A) Readings for market at 0.18°N , 34.3°E , normalised within 182 days (Materials & Methods). (B) Mean revenues and profits for 3,539 firms in Siaya County, indexed to January, along with smoothed activity normalized as in (A) and 95% CI for 16 markets within 5km from the firms (see Fig. S4). (C) Coefficient estimates from two activity regressions – market and non-market days – on monthly dummies. Vertical lines indicate 95% CI from market-day regression (263 markets; 1.9 market-day observations per month, marketplace and day of operation on average) Indexing as in (A) for data between 2018-22, excluding days whose reference average is affected by days between March 1, 2020 and June 1, 2020. Rainfall is monthly average across all marketplaces for the same period (22). Harvest seasons follow (23). (D) Marginal effects of rainfall shocks evaluated at zero from distributed lag model regressing market activity in April on monthly rainfall deviations from the 1998-2023 mean and their squares for the preceding six months. Sample as in (C). Standard errors clustered by year and rainfall gridcell (11km; 90% CI). (E) Sample as in (C). Shaded area indicates 95% CI from Epanechnikov-kernel. Grey bars indicate rainfall shock density.

Readings on non-market days also vary seasonally. This may partly reflect seasonal noise (e.g., clouds and their shadows appearing as brightness and colour differences) and, despite filtering and masking, affect the imagery more during rainy seasons. Also, markets could be active on non-market days during busy periods. Importantly, non-market day seasonal fluctuations are significantly smaller in magnitude, suggesting that the observed seasonality in market day activity reflects genuine changes in economic activity. Activity changes of a few percentage points in magnitude can be distinguished statistically with a sufficiently large panel.

Crop yields in the region depend on rainfall. Local staples respond negatively to excessive rain and potential waterlogging during germination, while maturing plants require more water (24). We investigate whether deviations from normal rainfall during the relatively water-scarce growing

season between October and April affect market activity in subsequent harvest periods (Fig. 3D). High rainfall during planting – three to four months before harvest – reduces harvest season market activity. High rainfall during the growing season has the opposite effect, until a reversal right before harvest, possibly related to the need to dry or transport crops. The effects are substantial: rainfall one standard deviation (SD) above the long-term mean in the preceding growing season correlates with approximately ten percentage points higher activity during the April harvest, a quarter of the usual seasonal amplitude.

While Fig. 3D considers the marginal effect of a relatively moderate rainfall deviation, the response to rainfall shocks in general is likely nonlinear (Fig. 3E). Extreme rains no longer increase and possibly decrease market activity.

Example application

We now present an application of economic monitoring in a remote and conflict-affected setting. In recent years, violent conflict has impacted livelihoods across Ethiopia, especially in the Tigray region (25). Violent conflict also hindered access to reliable information on economic conditions (26). In such a setting, remotely-sensed market activity can provide timely local information independent of ground conditions.

Periods of elevated conflict coincide with periods of lower market activity (Fig. 4A). Also, within the three selected regions, activity decreases were more sustained in some administrative zones than in others (Fig. 4B).

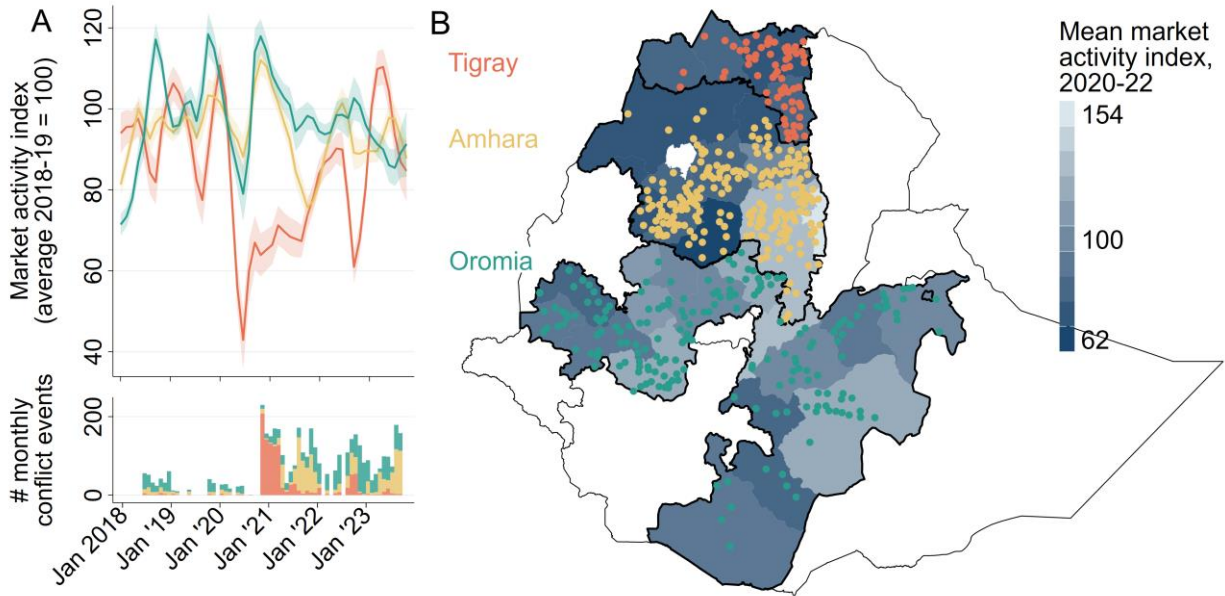


Fig. 4: Application of approach to country-wide monitoring in Ethiopia, 2018-23. (A) Market activity readings on market days averaged across 467 markets (coloured dots in (B)) in three Ethiopian regions, normalised to their 2018 average, along with counts of conflict events by region. (B) Map indicating marketplaces underlying activity measures in (A), with administrative zones shaded by average market activity index between 2018 and 2023. Administrative borders are taken from the FAO Global Administrative Unit Layers dataset, with some smaller neighbouring zones merged within the same region for easier interpretability.

Discussion

Monitoring marketplaces with satellite imagery provides unprecedented opportunities to track economic developments in remote and conflict-affected regions in near-real time and at high frequency. Our approach has broad applications. Policymakers could use the data to better target social assistance programs. Humanitarian actors could incorporate the measures in early-warning systems. Researchers could better understand the economic impacts of extreme events or policy changes in remote rural areas.

Across potential applications, the usefulness of our approach hinges on its ability to detect changes in economic conditions. Among other factors, this ability in turn depends on whether such changes manifest in changing market attendance, whether they are perceptible in imagery, and whether they are effectively extracted.

Regarding the first question, limited ground-based panels of economic activity in general and market attendance specifically inhibit our ability to go beyond the exercises in Figs. 3&4. For example, the relationship between market activity and local economic conditions may be non-linear. Correlating our activity measures with other high-frequency measures such as mobile phone data appears promising.

On the imagery side, we note that while PlanetScope's resolution, frequency, and global coverage uniquely enable our approach, challenges remain. Spatial misalignment between images, different spectral response functions between sensors, and imperfect cloud masking introduce idiosyncratic noise. Particularly in areas affected by cloud cover, this substantially affects market activity signals. Future sensors may allow for further improvements.

Regarding effective extraction, our method balances potential transferability across heterogeneous climatic and geographical contexts with the need to maintain reasonable computational loads. However, our approach can be locally tailored, especially when only a few markets or a specific period are of interest.

References

1. M. Ravallion, *The Economics of Poverty: History, Measurement, and Policy*. (Oxford University Press, 2016).
2. World Bank, “Poverty and Shared Prosperity 2020: Reversals of Fortune” (2020). doi.org/10.1596/978-1-4648-1602-4.
3. Editorial, A decades-long decline in extreme poverty has gone into reverse — here’s how to fix things. *Nature* **618**, 886 (2023).
4. P. Corral, A. Irwin, N. Krishnan, D. G. Mahler, T. Vishwanath. “Fragility and Conflict: On the Front Lines of the Fight against Poverty” (World Bank, 2020); <https://doi.org/10.1596/978-1-4648-1540-9>.
5. J. L. Alamy, J. Porciello, H. A. Tufan, J. Njuki, P. Winters, E. Mabaya, R. Coffman, M. June, Comment: Averting hunger in sub-Saharan Africa requires data and synthesis. *Nature* **584** (2020);
6. L. de Ligt, *Fairs and Markets in the Roman Empire*. (Brill, 1993).
7. P. Mukwaya, The dynamics and resilience of periodic markets in the Mt Elgon Region Uganda: a geographical perspective. *Rural-Urban Dynamics in the East African Mountains* 235-271 (2016).
8. G. Balineau, A. L. D. Bauer, M. Kessler, N. Madariaga, “Food Systems in Africa: Rethinking the Role of Markets” in *Africa Development Forum Series* (World Bank, 2021).
9. D. Donaldson, A. Storeygard, The View from Above: Applications of Satellite Data in Economics. *Journal of Economic Perspectives* **30** (2016).
10. M. Burke, A. Driscoll, D. B. Lobell, S. Ermon, Using satellite imagery to understand and promote sustainable development. *Science* **371**, 6535 (2021).
11. J. V. Henderson, A. Storeygard, D. N. Weil, Measuring economic growth from outer space. *American Economic Review* **102**, 2 (2012).
12. N. Jean, M. Burke, M. Xie, W. M. Davis, D. B. Lobell, S. Ermon, Combining satellite imagery and machine learning to predict poverty. *Science* 353, 6301 (2016).
13. S. Asher, T. Lunt, R. Matsuura, P. Novosad, Development Research at High Geographic Resolution: An Analysis of Night-Lights, Firms, and Poverty in India Using the SHRUG Open Data Platform. *The World Bank Economic Review* **35**, 4 (2021).
14. D. P. Roy, H. Huang, R. Houborg, V. S. Martins, A global analysis of the temporal availability of PlanetScope high spatial resolution multi-spectral imagery. *Remote Sensing of the Environment*. **264**, 112586 (2021).

15. O. Ghozatlou, M. Datcu, “Hybrid Gan and Spectral Angular Distance for Cloud Removal” in *2021 IEEE International Geoscience and Remote Sensing Symposium* (2021) pp. 2695-2698.
16. R. J. Bromley, R. Symanski, C. M. Good, The rationale of periodic markets. *Annals of the Association of American Geographers* **65**, 4 (1975).
17. L. F. Bergquist, M. Dinerstein, Competition and Entry in Agricultural Markets: Experimental Evidence from Kenya. *American Economic Review* **110**, 12 (2020).
18. USAID, Malawi Enhanced Market Analysis. [Online] (2018). [fews.net/sites/default/files/documents/reports/Malawi_EMA_Report_20180915_submitted_508compliant.pdf](https://www.fews.net/sites/default/files/documents/reports/Malawi_EMA_Report_20180915_submitted_508compliant.pdf) .
19. T. von Carnap, P. Christian, D. Jeong, A. Zwager, A. Tompsett, Route to Development: Impacts of Road Network Improvements on Agricultural Intensification in Mozambique (2020). [Trial registration] RIDIE-STUDY-ID-5f0d3682b0446
20. D. Egger, J. Haushofer, E. Miguel, M. Niehaus, M. Walker, General equilibrium effects of cash transfers: Experimental evidence from Kenya. *Econometrica* **90**, 6 (2022).
21. “Distribution of Farming Households by County” [Online] (Kenyan Ministry of Agriculture & Livestock Development, June 2024). <https://statistics.kilimo.go.ke/en/KenyafarmingHH/#>.
22. C. Funk, P. Peterson, M. Landsfeld, D. Pedreros, J. Verdin, S. Shukla, G. Husak, J. Rowland, L. Harrison, A. Hoell, J. Michaelsen, The climate hazards infrared precipitation with stations-a new environmental record for monitoring extremes. *Scientific Data* **2**, 150066 (2015).
- 23., “East Africa - crop calendars” [Online] (United States Department of Agriculture, 2024). https://ipad.fas.usda.gov/rssiws/al/crop_calendar/eafrica.aspx.
24. “Crop information.” [Online] (Food and Agriculture Organization of the United Nations, June 2024). <https://www.fao.org/land-water/databases-and-software/crop-information/en/>.
25. UN Office for the Coordination of Humanitarian Affairs, “*Humanitarian Response Plan Ethiopia*” (2022). <https://humanitarianaction.info/plan/1079>.
26. L. Weldegebriel, E Negash, J. Nyssen, D. B. Lobell, Eyes in the sky on Tigray, Ethiopia - Monitoring the impact of armed conflict on cultivated highlands using satellite imagery. *Science of Remote Sensing* **9**, e100133 (2024).
27. C. Raleigh, R. Kishi, A. Linke, “Political instability patterns are obscured by conflict dataset scope conditions, sources, and coding choices,” *Humanit. Soc. Sci. Commun.* **10** (no. 1), 1–17, 2023.
28. “Open spatial demographic data and research” [Online] (WorldPop, December 2020). <https://www.worldpop.org>.

29. OpenStreetMap contributors, OpenStreetMap place-of-worship layer (2024). <https://planet.osm.org> [Accessed - 12 Jun 2024].
30. Planet, “PlanetScope Scene Imagery Product Specification” (Planet Labs, 2022). https://assets.planet.com/docs/Planet_PSScene_Imagery_Product_Spec_letter_screen.pdf.
31. J. Kington, A. Collison, “Scene Level Normalization of Planet Dove Imagery” (Planet Labs, 2022). https://assets.planet.com/docs/scene_level_normalization_of_planet_dove_imagery.pdf.

Acknowledgments:

Funding: We gratefully acknowledge support from Riksbankens Jubileumsfond Infrastructure for Research Grant IN22-0041, STEG Small Research Grant 64 and the IGC project grant MOZ-22258. This work was also supported by an FSE postdoctoral fellowship to TC.

Author contributions:

Conceptualization: TC

Methodology: TC, RA, PD, AT

Investigation: TC, RA, PD, AT

Funding acquisition: TC, AT

Writing – original draft: TC

Writing – review & editing: TC, RA, PD, AT

Competing interests: Authors declare that they have no competing interests.

Supplementary Materials

Materials and Methods

Details of validation exercises and respective data collections

Details of application

Figs. S1 to S6

Tables S1 to S2

Data availability

Materials and Methods

Market detection

The following details how we get from a candidate market location to, if a market is confirmed, a shape outlining market areas and a time series of activity measures. Overall, our design choices within this approach reflect the desire for transferability across geographical contexts, the limitations of sparse ground truth data, and the need to maintain reasonable computational loads for the approach to be applied at scale.

While the satellite imagery would in principle allow for a true global screening for periodic appearance differences, such an approach would be prohibitively costly in terms of the necessary imagery and computation. For the purposes of the novel market maps in Kenya and Ethiopia, we therefore identified likely market locations from secondary information, such as pre-existing market maps or lists, visual interpretation of very high-resolution imagery, or by identifying areas of relatively higher population density within rural areas from gridded population datasets. Fig. S1 shows the set of locations where we applied our algorithm and highlights the locations where we

indeed confirmed a marketplace and that underlie the validation exercises. For each of the identified locations, we manually drew polygons around areas that could conceivably host a market – including built-up and adjacent areas but excluding waterbodies, forests and agricultural land. These polygons constitute our set of candidate locations.

We begin by identifying all PlanetScope Scenes that intersect with a given candidate location and, according to the provider, have less than 50 percent cloud cover across the whole image tile (287 to 637km²). For the purposes of this paper, we restricted our search to RGB imagery acquired after June 1, 2016 and before September 30, 2023 and downloaded orthorectified surface reflectance analytical data (Level 3B products) (30). For a typical location in, e.g., Western Kenya, this returns an initial sample of about 2,200 images. During the downloading stage, we make use of the provider’s pipeline to spatially align images using a cloud-free, post-2020 image as an anchor. This addresses distortions of the imagery due to varying sensor angles during acquisition.

We then process the imagery in Google Earth Engine. We first aim to identify whether a given candidate location indeed has areas of periodic appearance changes. We begin by masking each downloaded image with the provider’s ‘usable data mask’ (‘UDM2’) and filter the image collections to only include relatively clean images, covering at least 20 percent of the candidate location and being at least 80 percent shadow-, haze- and cloud-free across the whole image tile according to the imagery metadata (discarding about 10 percent of the initial sample). We furthermore exclude images that are acquired more than 30 minutes before or after the median acquisition time for each location to reduce the influence of differing lighting conditions (about 20 percent of the initial sample). We also filter out images with faulty colour representations, defined as images where the mean across pixel values within any of the red, green and blue bands is more than two standard deviations away from the mean of that statistic across all images (about 5 percent of the initial sample).

A complication stems from the two generations of satellites deployed by the provider during our sample period. Each generation operates with its own spectral response function, leading to the same colour on the ground being represented as different RGB values in images from either generation. If not properly addressed, these colour differences may be mistaken by our approach as changes in market activity. During the downloading stage, we follow the provider’s recommendation and spectrally align each image with Sentinel-2 imagery, harmonising colour representations in our imagery both across the two generations, and within each generation across individual satellites (31). Even after this adjustment, however, we observe ranges of the RGB band values to differ between the two imagery generations for the same location. For each location, we therefore create monthly target composites from images from the newer generation, to which we spectrally match images from both the older and newer generation. Specifically, we calculate 256 quantiles for each band in both individual old-generation images and the new-generation target composites and subsequently align distributions by scaling each quantile in the former to the value of the same quantile in the latter.

By inspecting images across geographical contexts, we furthermore find that brightness variation alone – as represented by differences within each of the red, green or blue colour bands – does not capture well the colour variation associated with marketplaces. We therefore calculate for each pixel a polar representation of its colour according to the following formulas:

$$\theta_1 = \arctan\left(\frac{\sqrt{red^2 + green^2}}{blue}\right); \quad \theta_2 = \arctan\left(\frac{green}{blue}\right)$$

θ_1 and θ_2 can be understood as angles between the individual bands identifying colours.

We then proceed to construct reference composites to serve as a comparison for each individual image. Our goal is a reference composite that for any given location and date resembles the appearance of that location when there is no market taking place. We therefore sample images that are temporally close – within ± 6 weeks of each image’s acquisition date – and maximise contrast

to potential market days by excluding images taken on the same day-of-week. From this initial sample, we select three copies of each of the two closest instances of every different day-of-week, two copies each of the next two closest instances and one copy each of the next two closest, giving us a maximum sample of

$$6 \text{ days of week} \times 2 \times (3 + 2 + 1) \frac{\text{images}}{\text{days of week}} = 72 \text{ images}$$

for the reference composite.

Parts of each image in this stack may be masked out because of cloud cover. Therefore, the effective number of images available for aggregation in each pixel will be lower than 72. We then construct an ‘interval mean’-composite from all pixels falling between the 40th and 60th percentile per band in the sample. In contrast to a canonical median composite, we found from inspection of the resulting difference images that this enlarged window helps address low-level noise coming from remaining spatial misalignment between images.

This way of selecting imagery for the reference composites performs satisfactorily in areas where clouds and their shadows are seasonal or generally covering large areas. Visual inspection, however, revealed that despite the multiple pre-processing steps, composites were often still noisy in areas where clouds typically occur in small patches of cumulus clouds, such as along tropical coasts. Here, a larger share of pixels in the stack is masked and unmasked pixels are more likely to be affected by noise from shadows or remaining cloud fragments. To address this, we identify in each reference composite from the first iteration those pixels that have less than 36 valid pixels to aggregate over. For these, we expand the sample by the next six temporally closest images per day-of-week that are not already included in the first iteration. While this expansion reduces temporal proximity, climates with such cloud patterns tend to see little seasonality, suggesting that composites from more temporally distant images can still provide a good approximation of a non-market day’s appearance.

We then match each individual image to its reference composite and calculate the absolute difference within each of the three colour bands as well as their ratios θ_1 and θ_2 . As our goal is to identify areas with periodic changes, we then calculate another interval-mean composite between the 40th and 60th percentile of these difference images sorted by day-of-week and converted to absolute values. In this representation, a pixel with a large value is one whose band value (red, green, blue, θ_1 , θ_2) is frequently different on a given day-of-week compared to other days.

We want to allow for both brightness and colour variation to indicate busier markets, and therefore multiply the maximum absolute difference across the RGB bands with the maximum absolute difference across the θ_1 , θ_2 bands. In this representation, a high value indicates a pixel where brightness and colour frequently differ from the reference composite.

Equipped with this representation of periodic differences across the extent of the candidate location – one difference image for each day of the week –, we then aim to extract areas with relatively high differences on any given day. We found that brightly reflecting surfaces, especially rooftops, regularly create artefacts in the difference images as their colour can change drastically when illuminated from different angles. These artefacts are sufficiently large and frequent to not be entirely addressed by our other averaging steps.

To reduce their influence, we perform two additional cleaning steps: first, we smooth out local outliers within the difference image using a 5-by-5 pixel median kernel. Second, since noise from bright rooftops is presumably uniformly distributed across days of the week – while the market signal is not – we subtract from each individual difference image an average of all other days of the week.

We then turn the cleaned pixel-level representations of periodic differences into contiguous areas. Noting that they lack a natural unit, we observe typical ranges of values across the derived

difference representations and define, based on inspection, a range of geometrically increasing threshold values as

$$\left\{ \left(\frac{t}{20} \right)^4 \mid t = 9, 10, 11, \dots, 34 \right\}.$$

We then extract all contiguous areas above each threshold, discarding those smaller than 50m² as these typically represent noise. Furthermore, we aim to eliminate spatial outliers – shapes that are identified far away from the main detected area in each location. For this, we identify for each candidate location the day-of-week and shape that is associated with the highest threshold value (a ‘peak’ in the difference image) and select for the same day the largest shape encircling this ‘peak’. We discard all shapes that do not intersect with this encompassing shape. This filtering step assumes that the area with the strongest signal represents the core area of a potential market and essentially restricts other possible market areas to be in the vicinity of the core.

In the Relevance and Validation section, we identified the threshold value at which we jointly maximise the share of actual markets that we detect and the share of markets among the detected shapes (Fig. 2A). Consequently, we discard candidate locations for which the lowest threshold value associated with any detected shape falls below the identified threshold of

$$\left(\frac{16}{20} \right)^4 = 0.41.$$

Within locations where the lowest threshold value exceeds this limit, we keep all detected shapes as possible market extents.

Activity tracking

Equipped with outlines of market extents under various threshold values, we turn to constructing measures of market activity. We here use all available images, including those on non-market days. The activity tracking follows much of the same logic as the market detection. We again construct temporally-relevant reference composites from relatively clean images, now also including images

that cover less than 20 percent of the overall candidate location, but at least 10 percent of the detected market area.

In the resulting difference images, we reduce noise from outlier pixels using a 3-by-3 pixel median kernel. For each image, we then derive the sum across pixels of the product of absolute brightness and colour differences within each of the previously detected market shapes, as well as their intersections.

The intersections allow us to identify areas where the market typically expands or contracts. Specifically, we rank the rings by the threshold value that defines them – sorting from rings nearest to the core of the market to rings further away – and construct for each ring the median activity reading on market days, as well as the 75th percentile reading on non-market days. We then define as the market fringe the smallest ring where median market day readings still exceed the 75th percentile of non-market day readings. The outer boundary of this ring defines the limits of the market area for which we construct the activity measures. To avoid very thin rings, we restrict the collection to intersections where the smaller of the areas in the intersection is less than 70 percent the size of the larger area. These areas can be associated with threshold values lower than the accuracy-maximising one from Fig. 2A.

The above procedure returns two outputs: First, the shapes of the identified market areas for each threshold level and day-of-week, and, second, a table where rows identify summed deviations in a given image and the identified preferred market extent.

Details of validation exercises and respective data collections

Figure 2 uses three sets of market maps for validation, each of them varying not just by country, but also by how they were collected and their intended purpose. The Kenyan dataset represents the marketplaces sampled for a study of trading behaviour (17) and was generously shared by the

authors. The authors reported having consulted with local government authorities for a market map but ultimately resorted to conducting their own, ground-based mapping.

The Malawian dataset originates from a policy report (18) and does not provide further detail on the approach for listing and selecting marketplaces. However, we noted that most locations represented in the map fall into relatively large settlements, such as district capitals.

The Mozambican dataset represents original data collected by the authors (19). As part of a larger study, enumerators were tasked to travel throughout a set of districts in the Nampula and Zambézia provinces along predefined routes. Market locations were identified from informant interviews as well as direct observation by enumerators during their travels. The sample used for the validation exercise includes only those marketplaces that enumerators found to be in operation during their surveys in 2021-23 and that had, according to local informants, a distinct market day. Enumerators were also tasked to photograph these locations on the ground, allowing the assessment of false negatives.

All validation maps come in the form of point coordinates either taken directly at the marketplace or in the surrounding village. To mimic a situation where market locations are not known ex-ante, we manually draw polygons around the entire settlement containing the marketplace as identified from the Google Maps basemap and subsequently apply the detection algorithm.

Across datasets, we repeatedly detect areas at high threshold levels on days where the dataset does not indicate a market day. In two cases each in Mozambique and Kenya, we detect areas only on a day other than the designated market day. In one case in Malawi, the validation data lists two market days (Mondays and Fridays), yet we detect areas only on Tuesdays and Saturdays. Since in all these cases the detected areas overlap directly with locations that appear similar to other listed marketplaces we detect in VHR imagery, we update the validation data to feature the

detected days instead of the initially designated ones. Fig. S6 illustrates the detected areas for these instances.

For the remaining exercises, we applied the algorithm above to an extensive set of candidate locations in Kenya and Ethiopia, which we identified based on historical censuses (1970 in Kenya, 2005 in Ethiopia) and manually from VHR imagery. While this procedure neither necessarily returns a complete market map, nor one derived from a consistent sampling frame, our sample is both geographically broad and dense. For detected markets, the closest other detected market on average lies 5km and 10km away in Kenya and Ethiopia, respectively.

Across analyses involving the activity data, we need to ensure that the readings – which have no naturally interpretable unit – are comparable over time and correctly weighted when aggregated, for example within regions. Intuitively, we aim to scale the readings such that within each marketplace and day of operation, their value equals 0 on average on non-market days and 100 on average on market days over a reference period. The reference period may differ by application.

A complication stems from the seasonal distribution not just of market activity, but also the number of readings. Our sample is dominated by images from times with relatively little cloud cover for a given location, whereas there are fewer observations during the rainy season. A simple average across all readings would therefore be biased towards the less cloudy seasons and not present a reference point that is comparable across locations with potentially differing seasons. We therefore use the available readings to construct a complete day-level time series of readings by applying an Epanechnikov kernel over a moving 90-day window, separately for both market day and non-market day readings as well as by sensor generation to address remaining level differences in activity readings. Our normalisation then subtracts the non-market day mean of these interpolated values over a given reference period and divides the thus differenced values by the mean of the interpolated market-day values.

For Fig. 3B, we use data generously shared by the research team of (20). This dataset of 3,539 non-agricultural firms was constructed to track long-term impacts of an earlier cash transfer experiment in Siaya County, Kenya. We excluded agricultural enterprises as their revenues were not recorded on a monthly basis. Each firm was surveyed once over the course of four months between January and May 2022 and asked to report their revenues and profits over the 30 days preceding the interview. Surveys were conducted in random order across a set of villages in the county, allowing us to construct a representative time series of economic activity. To protect respondent privacy, we only observe the month of their interview. Given the retrospective reporting, we reconstruct the time series of when revenues and profits were earned by randomly assigning each firm's stated values to any of the 30 days preceding the middle of the month of the interview, repeating that process 1,000 times and then taking the average per month of the assigned dates.

The activity data in Fig. 3B comes from the 16 detected markets that lie within 5km Euclidean distance of any of the firms' villages. To reduce noise, we exclude activity readings where the sun angle during acquisition is more than 14 degrees away from the median angle and images coming from tiles less than 90 percent cloud- and haze-free, according to the provider's metadata. We then normalise values according to the abovementioned procedure, averaging each image against the surrounding ± 182 days to maintain seasonality but purge year-to-year variance at the marketplace-market day level.

For Fig. 3C, we focus all detected markets in Kenya west of 36° longitude as the country's main agricultural region. We perform the same data cleaning and normalisation steps as for Fig. 3B, keeping data from January 2018 to December 2022 and excluding readings whose reference interpolations include readings acquired between March 1, 2020 and June 1, 2020, when normal seasonality patterns may have been affected by the COVID-19 pandemic. The point estimates

shown in the figure are from a regression of the activity measures – separately for market days and non-market days – on dummies for the month of observation, with standard errors clustered at the level of the marketplace and day-of-week of the area detected. The rainfall totals in the bottom part of the panel reflect the average rainfall over the four years in the sample across all markets in the sample when matched to monthly precipitation estimates (22). The definitions of harvest seasons follow (23).

For Fig. 3D, we select only observations in April as the peak month of the agricultural season where water is relatively more scarce. Here, we index market-day readings to the average interpolations in the proceedings 365 days so as to identify deviations from normal patterns. We derive rainfall shocks for each market and month as continuous deviations from the 1998-2023 mean in terms of standard deviations over that period. We then estimate the following distributed lag model including seven lagged periods and squared rainfall shocks.

$$mktAct_{t,i} = \beta_0 + \sum_{m=0}^6 (\beta_1 rainShock_{t-m} + \beta_2 rainShock_{t-m}^2) + \varepsilon_{t,i}$$

To account for spatial correlation in rainfall, we cluster standard errors at the level of the month and gridcell (11km resolution) where rainfall is measured. The effects reported in Fig. 3D are the marginal derivatives of the respective shocks at a shock value of zero and all other covariates at their respective means.

Details of application

Figure 4A shows the time series of the activity measure for three large regions of Ethiopia between 2018 and September 2023. When considering a time series this long, we found that despite our harmonisation procedure, activity readings differ between satellite generations. We therefore index the readings from the initial generation of PlanetScope imagery to their 2018 average per market, and subsequently index readings from the current generation so that at the regional level, the two

series have the same value on average where they overlap temporally, i.e. between November 2020 and May 2021.

We document patterns of conflict across the three regions in Fig. 4B based on counts of violent events (battles, explosions, protests, riots, violence against civilians) in the ACLED database (27).

Fig. 4C aggregates the activity measures of the detected markets to their administrative level – in this case a district. Districts are shaded according to the average monthly activity reading until September 2023, where darker districts have seen overall lower activity.

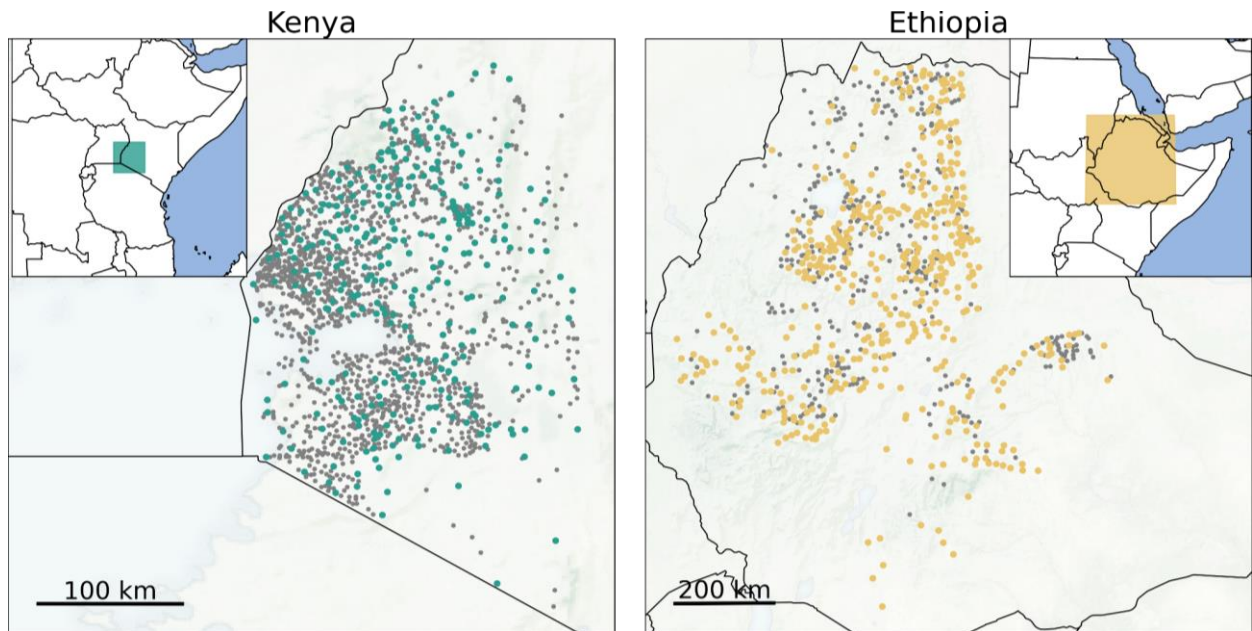


Fig. S1: Candidate locations and detected marketplaces in the Amhara, Oromia and Tigray regions of Ethiopia as well as in Kenya west of 36° longitude. Grey dots indicate locations where we applied our algorithm but did not detect periodic activity. We identified these ex-ante relatively likely market locations based on historical market maps (1970 in Kenya, 2007 in Ethiopia) as well as visual inspection of high-resolution satellite imagery. The coloured dots indicate locations where we confirmed a marketplace. The activity readings from these locations underlie the exercises in Figs. 3&4.

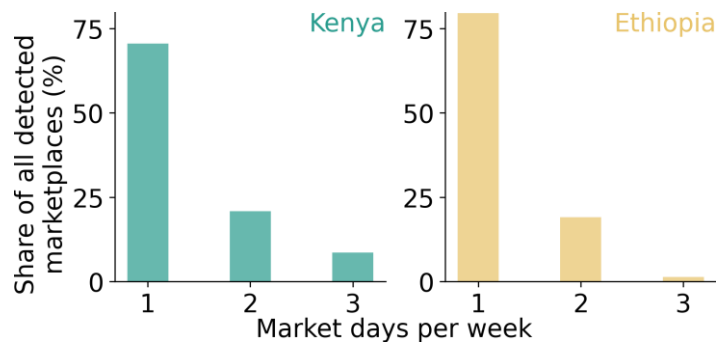


Fig. S2: Weekly market frequency in Kenya and Ethiopia. Bars indicate the share of detected markets with one, two or three market days in the samples from Ethiopia and Kenya.



Fig S3: Examples of detected market areas across four countries. (A) 14.35°N, 39.04°E; Ethiopia; Wednesday market **(B)** 11.6°N, 38.44°E; Ethiopia; Saturday **(C)** 0.23°N, 34.52°E; Kenya; Wednesday (green) and Saturday (red) **(D)** 1.62°S, 37.56°E; Kenya; Saturday **(E)** 16.2°S, 35.02°E; Malawi; Tuesday (green) and Saturday (red) **(F)** 15.02°S,

34.76°E; Malawi; Tuesday (G) 15.05°S, 40.31°E; Mozambique; Saturday (H) 13.96°S, 40.07°E; Mozambique; Saturday. Basemaps are from ESRI world imagery and show non-market days, except for panels (B) and (F), which are taken on the locations' respective market days.

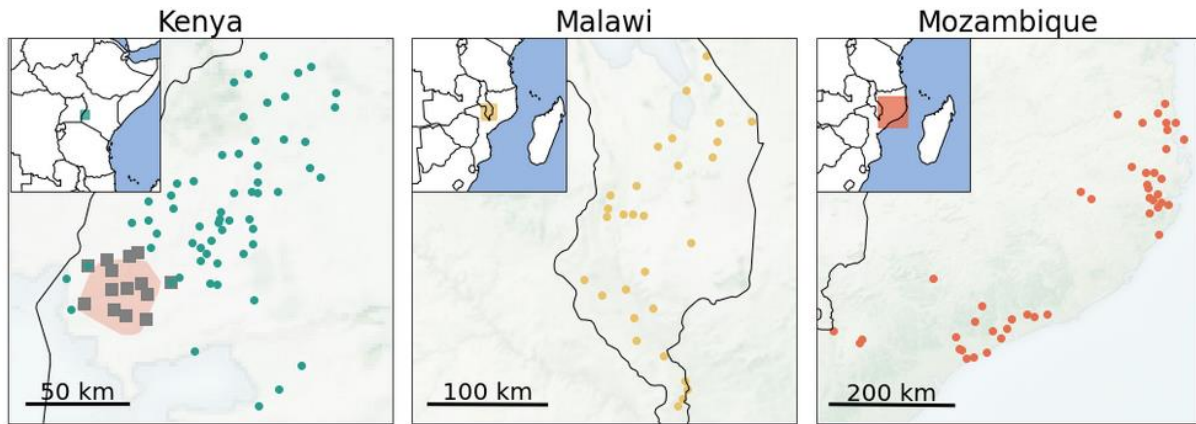


Fig. S4: Maps of validation datasets for market detection and activity tracking across three countries. Dots indicate locations of periodic marketplaces as recorded in reference datasets. In Kenya, the red polygon indicates the part of Siaya county where the survey of the firms in Fig. 3B took place. Grey squares indicate detected marketplaces within 5km of any firm.

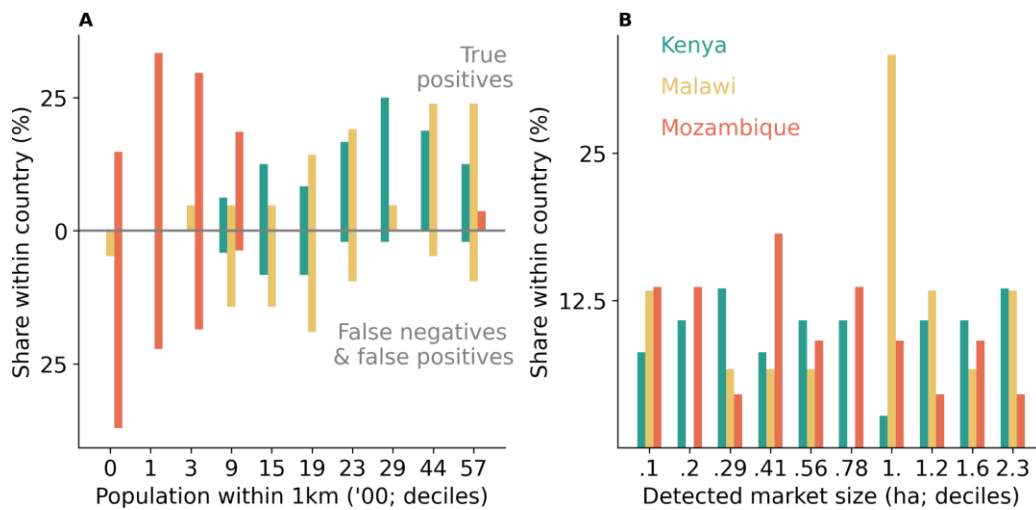


Fig. S5: Sizes of surrounding settlements and detected market areas for validation markets. (A) Population density (28) around validation locations with (top panel) and without (bottom panel) confirmed marketplaces, shaded by country. (B) Size of detected market areas in hectares by country.



Fig. S6: Validation markets with reassigned market days. For the shown locations, the validation data listed other market days than the sole ones on which we detect market activity, always in locations that appear highly similar to other marketplaces we detect. We therefore adjusted the validation data in these cases to reflect the high likelihood of falsely listed market days. (A) 1.03°N, 35.00°E; Kenya; Tuesday instead of Friday (B) 0.49°N, 34.84°E; Kenya; Monday instead of Friday (C) 15.13°S, 39.28°E; Malawi; Sunday instead of Tuesday (D) 16.97°S, 38.05°E; Malawi; Tuesday instead of Monday (E) 16.2°S, 35.02°E; Malawi; Tuesday and Saturday instead of Monday and Friday. Basemaps are from ESRI world imagery and show non-market days.

Supplementary Tables

| | | <u>Ethiopia</u> | | | | <u>Kenya</u> | | | |
|--------------------------------|--------|-----------------|------|------------------------|------|--------------|-------|------------------------|-------|
| | | <u>any</u> | | <u>Fri, Sat or Sun</u> | | <u>any</u> | | <u>Fri, Sat or Sun</u> | |
| Detected day: | | | | | | | | | |
| Number and share of | 50 | 3 | .5% | 1 | .3% | 34 | 3.7% | 30 | 6.5% |
| detected areas within ... | 100 | 16 | 2.4% | 10 | 2.8% | 58 | 6.4% | 46 | 10% |
| metres from religious | 250 | 50 | 7.5% | 29 | 8.2% | 104 | 11.4% | 74 | 15.9% |
| building | | | | | | | | | |
| Total number of detected areas | | 668 | | 355 | | 909 | | 464 | |
| (locations x market days) | | | | | | | | | |
| Distance to closest | Mean | | | 15.1 | | | | 8.8 | |
| recorded religious | | | | | | | | | |
| building (km) | Median | | | 10.5 | | | | 6.3 | |

Tab. S1: Number and share of detected markets in vicinity of known religious buildings. We identify churches and mosques from OpenStreetMap's place-of-worship layer (29). The distance is calculated as the straight line between the detected market and the closest religious centre in the area. Friday, Saturday and Sunday are chosen as days when religious services are held in each of the countries. We cannot reliably identify the denomination of each religious building and their associated days of worship.

| | | <u>Ethiopia</u> | <u>Kenya</u> |
|--|----------------------|-----------------|--------------|
| Detected market locations | | 545 | 644 |
| Locations with two detected market days | | 107 | 133 |
| Temporal distance between detected market days (days) | 3 (e.g., Mo & Th) | 86 | 86 |
| | 2 (e.g., Mo & We) | 9 | 15 |
| | 1 (e.g., Mo & Tu) | 12 | 32 |
| Spatial distance betw. detec- ted market area centroids (metres) | Mean | 140.4 | 276.5 |
| | Median | 26.1 | 34.8 |
| Size of candidate location (‘000 square metres) | Mean | 1,720 | 2,877 |
| | Median | 356 | 938 |

Tab. S2: Spatial and temporal proximity of detected market areas within candidate locations. Underlying samples in the two countries come from market detection exercises based on historical censuses and manual identification. We restrict to locations with two detected market days to avoid double-counting one potential false positive for locations with three detected market days in pairwise comparisons. Candidate locations are manually drawn polygons around populated areas to which the market detection algorithm is applied.

Data & code availability

We access the satellite imagery used in the paper under an academic research user agreement from the provider, which prevents us from making the imagery available directly. We have, however, publicly deposited all code that extracts information from the imagery as well as the derived datasets and the code producing the figures:
https://github.com/tillmannvc/market_activity_index